Constraining the Symmetron Model with the HUST-2020 Torsion Pendulum Experiment

Yuan-Ling Zhao,[1] Yu-Jie Tan,[1,*] Wen-Hao Wu,[1] Jie Luo,[2] and Cheng-Gang Shao[1]
[1]MOE Key Laboratory of Fundamental Physical Quantities Measurement and Hubei Key Laboratory of Gravitation and Quantum Physics, PGMF and School of Physics, Huazhong University of Science and Technology, Wuhan 430074, People's Republic of China
[2]School of Mechanical Engineering and Electronic Information, China University of Geosciences, Wuhan 430074, People's Republic of China

(Received 11 January 2022; revised 6 June 2022; accepted 8 September 2022; published 28 September 2022)

The search for dynamically screening the coupling between the scalar field and matter in high-density environment is achievable with the symmetron model. The high-accuracy and short-range gravity experiment is proposed to test the symmetron model. In this Letter, the data of the HUST-2020 torsion pendulum experiment testing the inverse-square law at submillimeter range is analyzed to constrain the symmetron model. The results show that the HUST-2020 experiment is uniquely sensitive to probe the symmetron model with a mass scale of $\mu = 7.2 \times 10^{-3}$ eV, and the self-coupling parameter $\lambda \lesssim 105$ is excluded at mass scale $M = 0.3$ TeV. Especially, at the dark energy scale $\mu = 2.4 \times 10^{-3}$ eV, the constraint at $M = 1.3$ TeV is improved by about 10 times the previous constraints on the torsion pendulum experiment.

DOI: 10.1103/PhysRevLett.129.141101

Overwhelming observational evidence has indicated that the expansion of the Universe is accelerating [1–4]. One possible explanation is the dark energy with negative pressure uniformly distributed in the Universe [5,6]. Although the standard lambda cold dark matter model is compatible with astronomical observation data, this model has some difficulties in explaining, for example, the cosmological constant problem [7] and the cosmic coincidence problem [8]. Therefore, theorists urgently need to find alternative models [6]. An intriguing extension is the scalar field dark energy model coupled with matter [9].

Since the fifth force has not been found on the laboratory and solar system scale, the coupled scalar field needs some screening mechanism to suppress the fifth force generated in the high-density region. Some screening mechanisms have been proposed so far, such as the chameleon mechanism [10–12], the Vainshtein mechanism [13–15], the K-mouflage mechanism [16–18], and the symmetron mechanism [19,20]. This Letter focuses on the symmetron mechanism, in which the coupling between the scalar field and matter is proportional to the vacuum expectation value (VEV) of scalar field depending on the background matter density. In the low-density region, the VEV becomes large and the symmetry is broken spontaneously, indicating that the field and matter are coupled at gravitational strength. In contrast, the VEV becomes small and the coupling is screened in the high-density region.

To further explore the properties of the dark energy screening mechanism, the symmetron model has been tested by atom interferometry experiments [21–23], gravity resonance spectroscopy [24,25], and accurate measurement experiments of the electron magnetic moment [26]. Also, some forecast constraints have been performed with the Casimir force experiment [27] and the next generation CANNEX experiment [28]. The Eöt-Wash torsion pendulum experiment [29], as a short-range gravity experiment, provides a complementary constraint of the parameter space [30].

In this Letter, we constrain the symmetron model with the HUST-2020 torsion pendulum experiment [31]. Since the regular flat-plate structures of the test and attraction masses are employed in this experiment, it is conducive to modeling the experimental geometry structure as a plate model, which is convenient to solve the one-dimensional symmetron field profile. We calculate the symmetron field profile between the torsion pendulum and the attractor, analyze the electrostatic shielding foil effect, and finally constrain the parameters of the symmetron model with the experimental data. We find that this experiment excludes a wider region of parameter spaces.

The symmetron model contains a symmetry-breaking potential $V(\phi)$ and a matter coupling $A(\phi)$, and the corresponding action can be written as [19,20]

$$S = \int \sqrt{-g} d^4x \left[-\frac{(\partial\phi)^2}{2} - V(\phi) \right] + S_m[A^2(\phi) g_{\mu\nu}], \quad (1)$$

where ϕ is the symmetron scalar field, $S_m[A^2(\phi) g_{\mu\nu}]$ is the coupling action of the scalar field and matter with $g_{\mu\nu}$ being the Einstein-frame metric. The scaler field equation of motion and the effective potential $V_{\text{eff}}(\phi, \rho)$ of the symmetron model can be derived as [30]

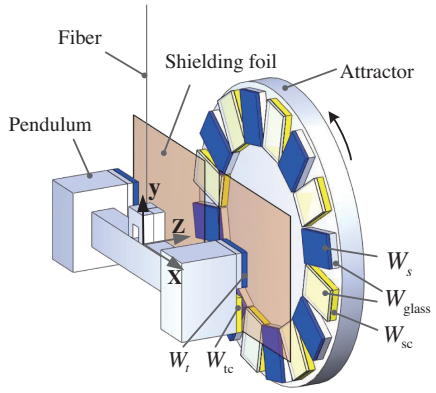

FIG. 1. Diagram of the HUST-2020 torsion pendulum experiment [31].

$$\nabla^2\phi = V_{\rm eff}(\phi,\rho)_{,\phi}, \qquad V_{\rm eff} = \frac{1}{2}\left(\frac{\rho}{M^2} - \mu^2\right)\phi^2 + \frac{\lambda}{4!}\phi^4, \tag{2}$$

where ρ is the background matter density, λ is the dimensionless coupling parameter, and μ and M are the mass scales. In the high-density region, namely $\rho > \mu^2 M^2$, the symmetry is not destroyed, and the effective potential has a minimum at $\phi = 0$ eV, indicating that the coupling between the field and matter is nearly vanished. Nevertheless, in the low-density region, such as in vacuum $\rho < \mu^2 M^2$, the symmetry is spontaneously broken and two local minima of the potential are generated, corresponding to two nonzero $\phi_V = \pm\sqrt{6(\mu^2 - \rho/M^2)/\lambda}$. Without loss of generality, we take ϕ_V as positive. In this case, the field and matter are coupled at gravitational strength, mediating a large symmetron force. For the symmetron with different mass scales μ, the HUST-2020 experiment can provide the constraint of the symmetron model parameters M-λ.

The HUST-2020 experiment is described in detail in [31]. A brief review is provided here, and the structural diagram can refer to Fig. 1. The I-shaped pendulum, including $14.6 \times 0.2 \times 12.0$ mm^3 tungsten test masses W_t and $14.6 \times 0.3 \times 12.0$ mm^3 tungsten gravitational compensation masses $W_{\rm tc}$, is symmetrical on both sides and directly opposite to the attractor. The attractor is eightfold symmetric, and comprises eight $17.6 \times 0.2 \times 11.4$ mm^3 tungsten attraction masses W_s, attached to the surface of the equal-area glass masses $W_{\rm glass}$, and eight $17.6 \times 0.4 \times 11.4$ mm^3 glass masses, attached to the surface of the equal-area tungsten gravitational compensation masses $W_{\rm sc}$. The attractor is rotated around the horizontal z axis to produce the density modulation. A 30-μm-thick electrostatic shielding foil is inserted between the test mass and the attraction mass to prevent electrostatic disturbance. The densities of the glass plate, tungsten plates, and foil are $\rho_b = 2.5$ g/cm^3, $\rho_w = 18.9$ g/cm^3, and $\rho_s = 8.4$ g/cm^3 respectively. The entire experimental system is placed in a vacuum chamber with a pressure of about 10^{-5} Pa. In particular, the compensation masses added in this experiment can effectively offset the Newtonian torque, realizing a "null" measurement. The violating torque is measured at different test-attraction mass separations as $d_0 = 210$ μm and 295 μm, in which the separation between the test mass and the foil is 90 μm, and the experimental resolution of the torque at 1σ level is 1.0×10^{-17} N $\cdot$ m.

Because of the density modulation adopted in the HUST-2020 experiment, there mainly exist two experimental configurations: the tungsten test mass and the tungsten (or glass) attraction mass are placed on both sides of the foil. This sandwich like structure can be easily modeled as a three-plate model. To analyze the constraint of the HUST-2020 experiment on the symmetron model, it is important to calculate the symmetron torque difference in the three-plate model. However, considering that it is very complicated to directly solve the symmetron field profile as well as torque difference in the three-plate model, we convert it into calculating the symmetron torque difference in the two-plate model of test mass and attraction mass, and further analyzing the influence of the electrostatic shielding foil, which is considered as a correction on the symmetron torque difference.

The two-plate model mainly involves two configurations: the tungsten test mass facing the tungsten or the glass attraction mass. These correspond to two different symmetron field profiles, illustrated in Fig. 2(a). The red dashed line represents the symmetric field profile for the tungsten-to-tungsten plate, and the red solid line represents the

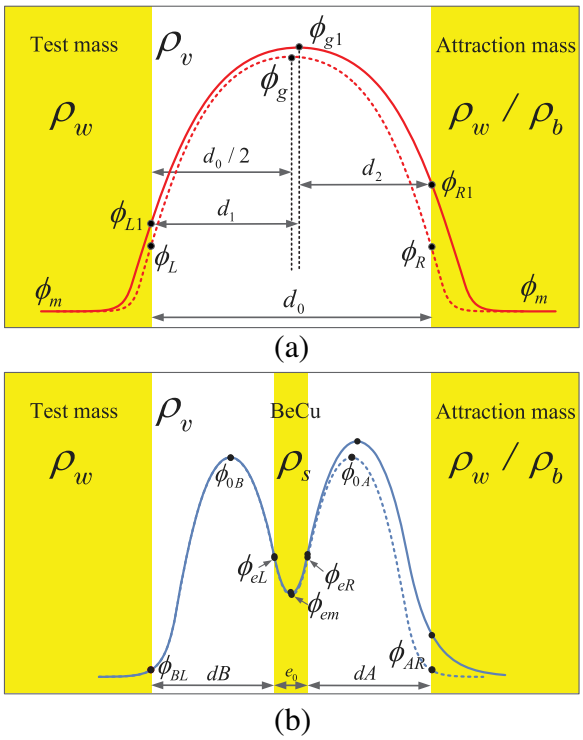

FIG. 2. Sketch of symmetron field profiles for the two-plate model (a) and the three-plate model (b). The densities of the tungsten, glass, foil, and vacuum regions are expressed as ρ_w, ρ_b, ρ_s, and ρ_v, respectively.

asymmetric field profile for the tungsten-to-glass plate. As symmetric field profile is a special case of asymmetric field profile, we take the asymmetric field profile as an example to analyze. Based on the plate model, Eq. (2) can be rewritten as a one-dimensional form [32,33]:

$$\left(\frac{d\phi}{dz}\right)^2\Big|_{z_i} - \left(\frac{d\phi}{dz}\right)^2\Big|_{z_j} = 2V_{\rm eff}(\phi_i,\rho) - 2V_{\rm eff}(\phi_j,\rho), \quad (3)$$

where $\phi_i \equiv \phi(z_i)$ and $\phi_j \equiv \phi(z_j)$, respectively, represent the symmetron field values at z_i and z_j. ϕ_m and ϕ_{L1} represent the local minimum of the symmetron field inside the test mass and the surface field value on the test mass, respectively. ϕ_{g1} represents the local maximum of the field between both plates. From Eq. (3), both of the equations of motion in the plate interval $[\phi_m, \phi_{L1}]$ and vacuum interval $[\phi_{L1}, \phi_{g1}]$ can be obtained, and further ϕ_{g1} can be derived as

$$\begin{aligned}&\phi_{g1}\\ &= \left[\phi_V^2 - \sqrt{\phi_V^4 - \frac{12}{\lambda}\left(\frac{\rho_w-\rho_v}{M^2}\phi_{L1}^2 - \frac{\rho_w-\mu^2M^2}{M^2}\phi_m^2\right) + \phi_m^4}\right]^{1/2}\\ &\equiv \phi_{\rm max}[\phi_m, \phi_{L1}, \rho_w]. \end{aligned} \quad (4)$$

Conversely, the field value ϕ_{L1} can be obtained with $\phi_{L1} \equiv \phi_{\rm mid}[\phi_m, \phi_{g1}, \rho_w]$. From Eq. (3), the equation of motion in the vacuum interval $[\phi, \phi_{g1}]$ can be given. Integrating the field value from ϕ to ϕ_{g1}, one can obtain Δz as [30]

$$\begin{aligned}\Delta z &= \frac{1}{\mu_{\rm vac}}\left(1 - \frac{\phi_{g1}^2}{2\phi_V^2}\right)^{-1/2}\left[F\left(\frac{\pi}{2}, k\right) - F\left(\sin^{-1}\frac{\phi}{\phi_{g1}}, k\right)\right]\\ &\equiv \Delta z[\phi, \phi_{g1}], \end{aligned} \quad (5)$$

where $\mu_{\rm vac}^2 \equiv \mu^2 - \rho_v/M^2$, $k \equiv \phi_{g1}^2/(2\phi_V^2 - \phi_{g1}^2)$, and $F(\theta, m) = \int_0^\theta (1 - m\sin\theta^2)^{-1/2} d\theta$ is the elliptic integral. The asymmetric field profile can be solved by the dichotomy algorithm. Guess an arbitrary field value ϕ_{L1}, based on Eqs. (4) and (5), the field value ϕ_{g1} and the distance d_1 from ϕ_{L1} to ϕ_{g1} can be determined, respectively. Since the distance $d_2 = d_0 - d_1 = \Delta z[\phi_{R1}, \phi_{g1}]$, one can obtain the field value ϕ_{R1} and the slope ϕ'_{R1}. Then, we deduce the slope $\tilde{\phi}'_{R1}$ with a guess field value $\tilde{\phi}_{R1}$ on the surface of the attraction mass. If the iteration conditions $|\phi_{R1} - \tilde{\phi}_{R1}| < 10^{-21}$ eV and $|\phi'_{R1} - \tilde{\phi}'_{R1}| < 10^{-21}$ eV $\cdot$ cm^{-1} are satisfied, the correct value of ϕ_{L1} is found, as well as the entire symmetron field profile. A similar analysis can be performed to solve the symmetric symmetron field profile between the two plates with same density. According to the mass blocks used in this experiment being a regular flat-plate structure, the symmetron force per unit area in the z direction can be expressed as [32]

$$F_\phi = -c^2\frac{\rho_w}{2M^2}[\phi^2(d+D) - \phi^2(d)]. \quad (6)$$

Here, ρ_w is the density of the test mass, and D is the thickness of the test mass plate. $\phi(d+D)$ and $\phi(d)$, respectively, denote the symmetron field values on the left and right surfaces of the test mass plate. Based on the density modulation adopted in this experiment, the symmetron torque difference between the two configurations in the two-plate model can be expressed as

$$\delta\tau = c^2\frac{Sl\rho_w}{2M^2}(\phi_{L1}^2 - \phi_L^2). \quad (7)$$

Here, S is the area of the test mass, l is the arm length, and $\phi_{L1}(\phi_L)$ represents the field value on the right surface of the test mass plate for the tungsten plate facing the glass (tungsten) plate.

When a foil is inserted between the test mass and the attraction mass, the experimental structure should be modeled as a three-plate model. Compared with the case of the two-plate model, the symmetron field profile is different, illustrated in Fig. 2(b). The blue dashed line represents the field profile of the case that the test mass and attraction mass are tungsten to tungsten. The field values of the critical points are denoted as ϕ_{BL}, ϕ_{0B}, ϕ_{eL}, ϕ_{em}, ϕ_{eR}, ϕ_{0A}, and ϕ_{AR}. ϕ_{BL} and ϕ_{AR}, respectively, and represent the surface field values on the test and attraction masses. ϕ_{0B} (ϕ_{0A}) represents the local maximum of the field between the test (attraction) mass and foil. ϕ_{eL} and ϕ_{eR} represent the surface field values on the foil, and ϕ_{em} represents the local minimum of the field inside the foil. The blue solid line represents the field profile of the case that the test and attraction masses are tungsten to glass. The difference of the two field profiles corresponding to both configurations is weak in the areas far from the attraction mass. The symmetron torque difference between both configurations is $\delta\tau_{\rm foil}$. Similarly, for the two-plate model, the torque difference denotes as $\delta\tau_{\text{no-foil}}$. Therefore, the influence of the foil on torque difference defines as $f \equiv \delta\tau_{\rm foil}/\delta\tau_{\text{no-foil}}$.

In the HUST-2020 experiment, when the attractor is rotated from tungsten to glass, the reduction of the attraction-mass density is $\rho_w - \rho_b$. To present an approximate analytical calculation, we regard the reduced amount of the attraction-mass density as a small amount $\delta_\rho\rho_w$, and the field profile in this case changes slightly compared with the case of the three-plate configuration of the tungsten test mass, the foil and the tungsten attraction mass. Thus, the field values of the critical points are

$$\begin{aligned}&\phi_{BL\delta} = \phi_{BL}(1+\delta_1), \qquad \phi_{0B\delta} = \phi_{0B}(1+\delta_2),\\ &\phi_{eL\delta} = \phi_{eL}(1+\delta_3), \qquad \phi_{em\delta} = \phi_{em}(1+\delta),\\ &\phi_{eR\delta} = \phi_{eR}(1+\delta_4), \qquad \phi_{0A\delta} = \phi_{0A}(1+\delta_5),\\ &\phi_{AR\delta} = \phi_{AR}(1+\delta_6), \end{aligned} \quad (8)$$

with $\delta \sim \delta_6$ representing the relative increment of the field values for the three-plate model, where the test and

attraction masses are with the same density. The notation is introduced as $k_i \equiv \delta_i/\delta (i = 1, 2...6, \rho)$. Making a first-order Taylor expansion of $\phi_{BL\delta} = \phi_{\rm mid}[0, \phi_{0B\delta}, \rho_w]$ at $\phi_{BL} = \phi_{\rm mid}[0, \phi_{0B}, \rho_w]$, one gets the relationship

$$k_1 = \frac{\partial \phi_{\rm mid}[0, \phi_{0B}, \rho_w]}{\partial \phi_{0B}} \frac{\phi_{0B}}{\phi_{BL}} k_2. \tag{9}$$

Similarly, we determine the relationship between k_2 and k_3. Since the distance dB between the test mass and the foil is a fixed value $dB = \Delta z[\phi_{BL\delta}, \phi_{0B\delta}] + \Delta z[\phi_{eL\delta}, \phi_{0B\delta}]$ can be described as a Taylor expansion at $dB = \Delta z[\phi_{BL}, \phi_{0B}] + \Delta z[\phi_{eL}, \phi_{0B}]$, and the relationship of k_1, k_2, and k_3 are then derived. Further, k_3 can be determined and is related to the field values of the three-plate model with the test and attraction masses with the same density. Similarly, the dependent relationships of k_4, k_5, k_6, and k_ρ on k_3 can be derived. Thus, $\delta\tau_{\rm foil}$ expresses as

$$\delta\tau_{\rm foil} = c^2 \frac{Sl\rho_w}{2M^2} \frac{2\phi_{BL}^2 k_1}{k_\rho \rho_w}. \tag{10}$$

For the two-plate model, when the attraction-mass density reduces by $\delta_\rho \rho_w$, the field values of critical points ϕ_L, ϕ_g, and ϕ_R also change, as well as the relative increments δ_1', δ', and δ_2'. ϕ_L and ϕ_R represent the surface field values on the test and attraction masses, respectively. ϕ_g is the local maximum of the symmetron field in vacuum. A similar analytical calculation can be performed to solve $\delta\tau_{\text{no-foil}}$. Finally, the influence of the foil on the torque difference can be obtained as

$$f = \frac{\phi_{BL}^2}{\phi_L^2} \frac{k_1 k_\rho'}{k_\rho k_1'}, \tag{11}$$

with $k_\rho' \equiv \delta_\rho/\delta'$ and $k_1' \equiv \delta_1'/\delta'$. Besides the above analytical calculations, the numerical method, which has been presented in detail in [34] to analyze the constraints of the chameleon model with the short-range gravity experiment, should be adopted to solve the symmetron field profile with the test and attraction masses with the same density. We denote the calculation method of foil influence as a kind of "semianalytical" method. The detailed calculation of the foil influence is in the Supplemental Material [35].

Based on the semianalytical results in Eq. (11), the foil influences at $\mu = 7.2 \times 10^{-3}$ eV for different distances d_0 are shown in Fig. 3. The results show that when the dimensionless value of $m_0 \times e_0$ is close to zero, the foil is equivalent to a sufficiently thin plate, which has an extremely weak influence on the symmetron torque difference, and the foil influence is $f \approx 1$; as $m_0 \times e_0$ increases gradually, about in the interval $0 < m_0 \times e_0 < 4.5$, the foil influence satisfies $f > 1$, and its maximum value is approximate to 6. The rationality of this interesting phenomenon will be analyzed in detail in the following paragraph; when $m_0 \times e_0$ increases to a large enough value, the foil is equivalent to a thick plate, indicating a strong screening effect on the torque difference, and the foil influence satisfies $f \ll 1$. In addition, the numerical method is also adopted to calculate the foil influence, and the results agree well with the semianalytical method, shown in Fig. 3. Similarly, one can calculate the foil influence of other mass scales μ, and can obtain similar properties of foil influence f.

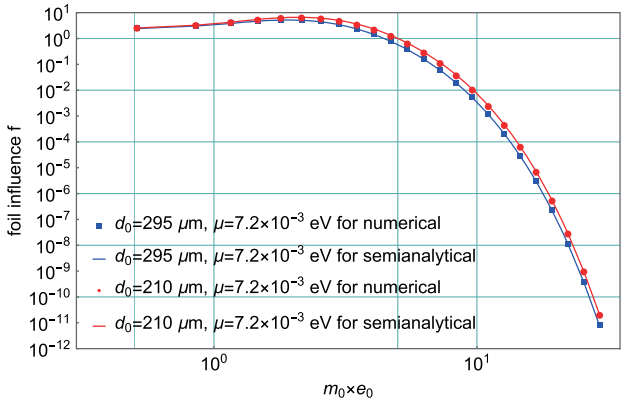

FIG. 3. The influence of the foil on symmetron torque difference. The dots and lines represent the results of numerical and semianalytical calculations, respectively. Here, the self-coupling $\lambda = 1$, and $m_0^2 = \rho_s/M^2 - \mu^2$.

To analyze the rationality on the enhancement effect of the foil influence in the interval about $0 < m_0 \times e_0 < 4.5$, the limit case is constructed by making the value of $m_0 \times e_0$ close to zero. We choose $\mu = 7.2 \times 10^{-3}$ eV, $M = 1/4$ TeV, $\lambda = 1$, and the experimental distance $d_0 = 210$ μm. The semianalytical method is adopted to calculate the foil influence for the foil thickness e_0 in the interval 10^{-12} cm $\sim 10^{-10}$ cm, and the result can be approximately fitted as $f \approx \exp(14 m_0 e_0/5)$. For $e_0 \to 0$, one can obtain the foil influence $f > 1$ and the slope $f' > 0$, demonstrating that it does have an enhancement effect. In addition, one can understand this phenomenon from a more intuitive perspective. Generally, when a thin foil is inserted between the two plates, the foil will screen the symmetron field profile. However, due to the density modulation adopted in the HUST-2020 experiment, we need to consider the influence of the foil on the symmetron torque difference. Considering the two cases that the test mass and the attraction mass are tungsten to tungsten and tungsten to glass, the foil is inserted between the two plates in these two cases. In the interval about $0 < m_0 \times e_0 < 4.5$, we note that the screening effect of the foil in the tungsten-to-glass case is weaker than that of the tungsten-to-tungsten case. This, to some extent, explains why the foil influence is $f > 1$ in this interval. The more detailed analysis on the enhancement effect of the foil influence is given in the Supplemental Material [35].

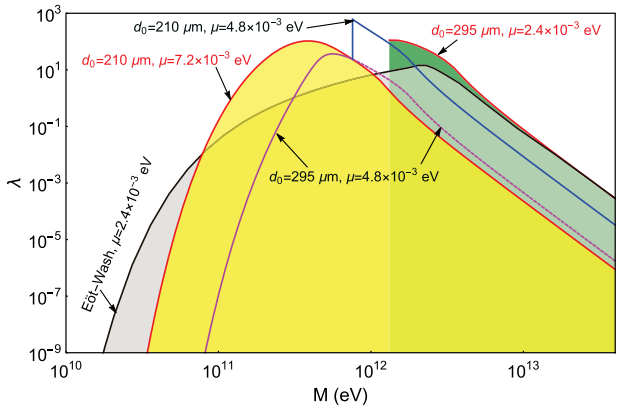

FIG. 4. The constraint of the torsion pendulum experiment on symmetron model. For the HUST-2020 experiment, the yellow and green regions are excluded, respectively, for $\mu = 7.2 \times 10^{-3}$ eV and $\mu = 2.4 \times 10^{-3}$ eV; a combination of the blue (solid) and purple (both solid and dashed) curves gives lower bounds on λ for $\mu = 4.8 \times 10^{-3}$ eV. The gray shaded region surrounded by black curve is excluded for $\mu = 2.4 \times 10^{-3}$ eV by Eöt-Wash experiment [30].

Based on the above analysis, the symmetron torque in the HUST-2020 experiment can be calculated as $\delta\tau_{\rm tot} = \delta\tau \times f$, and one can constrain the symmetron model with the experimental data. Generally, the study of the symmetron field profile between two plates is limited by a minimum distance $\Delta z_{\rm min}$. When the experimental distance d between these two plates is less than the minimum distance $\Delta z_{\rm min}$, the symmetron field is near zero everywhere, and the experiment will fail to constrain the symmetron model [30]. $\Delta z_{\rm min}$ can be determined by taking $\phi = \phi_L$ and the limit $\phi_g \to 0$ in Eq. (5), approximately expressed by $\Delta z_{\rm min} \approx \pi/\sqrt{\mu^2 - \rho_v/M^2}$. Therefore, for some certain mass scale μ, $d > \Delta z_{\rm min}$ is satisfied at all M of interest; while for μ with little values, $d > \Delta z_{\rm min}$ is only satisfied at a certain range of M. This leads to the curves of the constraint being "truncated." In this Letter, we adopt the experiment performed at $d_0 = 210$ μm, 295 μm to analyze the constraint of the symmetron model. Combined with the resolution level of the torque, the constraints of the HUST-2020 experiment on symmetron model are shown in Fig. 4. The current strongest constraint on $\mu = 7.2 \times 10^{-3}$ eV is obtained by analyzing the experimental data with $d_0 = 210$ μm, finding that the self-coupling parameter $\lambda \lesssim 105$ is excluded for the mass scale $M = 0.3$ TeV. Combining the experimental data with $d_0 = 295$ μm, at the dark energy scale $\mu = 2.4 \times 10^{-3}$ eV, the self-coupling parameter $\lambda \lesssim 112$ is excluded for $M = 1.3$ TeV, which is improved by about 10 times from that of the Eöt-Wash experiment [30]. Because of the truncation phenomenon, this experiment can only constrain the symmetron model at a certain range of M. Moreover, a combined analysis of the experiments with $d_0 = 210$ μm and $d_0 = 295$ μm has been performed to constrain the symmetron model of the mass scale $\mu = 4.8 \times 10^{-3}$ eV.

The symmetron model is one of the most successful screening mechanism models, which helps with understanding the accelerating expansion of the Universe. Therefore, it is extremely significant to place constraints on the symmetron model. We constrain the symmetron model with different mass scales μ by combining with the HUST-2020 experimental data. As the special design of density modulation is adopted in the HUST-2020 experiment, we found an interesting phenomenon that the symmetron torque signal in this experiment is enhanced in some certain interval of $m_0 \times e_0$. This is unique and useful for designing the test of the symmetron model in the future. In addition, we are currently running a new experiment of the HUST torsion pendulum in the submillimeter range [36] that may further provide meaningful constraints on the symmetron dark energy model.

This work is supported by the National Natural Science Foundation of China (Grants No. 12175076 and 11925503), Guangdong Major Project of Basic and Applied Basic Research (Grant No. 2019B030302001), and the Fundamental Research Funds for the Central Universities, HUST: 2172019kfyRCPY029.

*Corresponding author.
yjtan@hust.edu.cn

[1] A. G. Riess, A. V. Filippenko, P. Challis *et al.*, Astron. J. **116**, 1009 (1998).
[2] S. Perlmutter, G. Aldering, M. Della Valle *et al.*, Nature (London) **391**, 51 (1998).
[3] A. Balbi, P. Ade, J. Bock, J. Borrill, A. Boscaleri *et al.*, Astrophys. J. Lett. **545**, L1 (2000).
[4] D. J. Eisenstein, I. Zehavi, D. W. Hogg *et al.*, Astrophys. J. **633**, 560 (2005).
[5] J. A. Frieman, M. S. Turner, and D. Huterer, Annu. Rev. Astron. Astrophys. **46**, 385 (2008).
[6] E. J Copeland, M. Sami, and S. Tsujikawa, Int. J. Mod. Phys. D **15**, 1753 (2006).
[7] S. Weinberg, Rev. Mod. Phys. **61**, 1 (1989).
[8] I. Zlatev, L. Wang, and P. J. Steinhardt, Phys. Rev. Lett. **82**, 896 (1999).
[9] A. Joyce, B. Jain, J. Khoury, and M. Trodden, Phys. Rep. **568**, 1 (2015).
[10] J. Khoury and A. Weltman, Phys. Rev. Lett. **93**, 171104 (2004).
[11] J. Khoury and A. Weltman, Phys. Rev. D **69**, 044026 (2004).
[12] P. Brax, C. van de Bruck, A.-C. Davis, J. Khoury, and A. Weltman, Phys. Rev. D **70**, 123518 (2004).
[13] N. Arkani-Hamed, H. Georgi, and M. D. Schwartz, Ann. Phys. (Amsterdam) **305**, 96 (2003).
[14] C. Deffayet, G. Dvali, G. Gabadadze, and A. Vainshtein, Phys. Rev. D **65**, 044026 (2002).
[15] A. I. Vainshtein, Phys. Lett. B **39**, 393 (1972).

[16] E. Babichev, C. Deffayet, and R. Ziour, Int. J. Mod. Phys. D **18**, 2147 (2009).
[17] P. Brax, C. Burrage, and A.-C. Davis, J. Cosmol. Astropart. Phys. 01 (2013) 020.
[18] P. Brax and P. Valageas, Phys. Rev. D **90**, 123521 (2014).
[19] K. Hinterbichler and J. Khoury, Phys. Rev. Lett. **104**, 231301 (2010).
[20] K. Hinterbichler, J. Khoury, A. Levy, and A. Matas, Phys. Rev. D **84**, 103521 (2011).
[21] C. Burrage, A. Kuribayashi-Coleman, J. Stevenson, and B. Thrussell, J. Cosmol. Astropart. Phys. 12 (2016) 041.
[22] M. Jaffe, P. Haslinger, V. Xu, P. Hamilton, A. Upadhye, B. Elder, J. Khoury, and H. Müller, Nat. Phys. **13**, 938 (2017).
[23] D. O. Sabulsky, I. Dutta, E. A. Hinds, B. Elder, C. Burrage, and E. J. Copeland, Phys. Rev. Lett. **123**, 061102 (2019).
[24] G. Cronenberg, P. Brax, H. Filter, P. Geltenbort, T. Jenke, G. Pignol, M. Pitschmann, M. Thalhammer, and H. Abele, Nat. Phys. **14**, 1022 (2018).
[25] T. Jenke, J. Bosina, J. Micko, M. Pitschmann, R. Sedmik, and H. Abele, Eur. Phys. J. Special Topics **230**, 1131 (2021).
[26] P. Brax, A.-C. Davis, B. Elder, and L. K. Wong, Phys. Rev. D **97**, 084050 (2018).
[27] B. Elder, V. Vardanyan, Y. Akrami, P. Brax, A.-C. Davis, and R. S. Decca, Phys. Rev. D **101**, 064065 (2020).
[28] R. I. P. Sedmik and M. Pitschmann, Universe **7**, 234 (2021).
[29] D. J. Kapner, T. S. Cook, E. G. Adelberger, J. H. Gundlach, B. R. Heckel, C. D. Hoyle, and H. E. Swanson, Phys. Rev. Lett. **98**, 021101 (2007).
[30] A. Upadhye, Phys. Rev. Lett. **110**, 031301 (2013).
[31] W.-H. Tan, A.-B. Du, W.-C. Dong, S.-Q. Yang, C.-G. Shao, S.-G. Guan *et al.*, Phys. Rev. Lett. **124**, 051301 (2020).
[32] M. Pitschmann, Phys. Rev. D **103**, 084013 (2021).
[33] P. Brax and M. Pitschmann, Phys. Rev. D **97**, 064015 (2018).
[34] Y.-L. Zhao, Y.-J. Tan, W.-H. Wu, J. Luo, and C.-G. Shao, Phys. Rev. D **103**, 104005 (2021).
[35] See Supplemental Material at http://link.aps.org/supplemental/10.1103/PhysRevLett.129.141101 for the calculation method and the rationality on the enhancement effect of the foil influence.
[36] A.-B. Du, W.-H. Tan, W.-C. Dong, and H. Huang, L. Zhu, Y.-J. Tan, C.-G. Shao, S.-Q. Yang, and J. Luo, Classical Quantum Gravity **39**, 105008 (2022).